INSTITUTE FOR FUSION STUDIES

DE-FG03-96ER-54346-753 IFSR #753

Evolution of Toroidal Alfvén Eigenmode Instability in TFTR

K.L. WONG, R. MAJESKI, M. PETROV,[a] J.H. ROGERS,
G. SCHILLING, J.R. WILSON
Plasma Physics Laboratory
Princeton University
Princeton, NJ 08543
H.L. BERK, B.N. BREIZMAN, M. PEKKER, and H.V. WONG
Institute for Fusion Studies
The University of Texas at Austin
Austin, Texas 78712 USA

[a]Permanent address: A.F. Ioffe Physical-Technical Inst., St. Petersburg 194021, Russia

July 1996

THE UNIVERSITY OF TEXAS

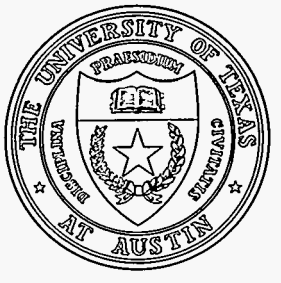

AUSTIN

Evolution of Toroidal Alfvén Eigenmode Instability in TFTR

K.L. Wong, R. Majeski, M. Petrov,[a] J.H. Rogers, G. Schilling, and J.R. Wilson

Plasma Physics Laboratory, Princeton University, Princeton, New Jersey 08543

and

H.L. Berk, B.N. Breizman, M. Pekker, and H.V. Wong

Institute for Fusion Studies, The University of Texas at Austin

Austin, Texas 78712 USA

Abstract

The nonlinear behavior of the Toroidal Alfvén Eigenmode (TAE) driven unstable by energetic ions in TFTR [Phys. Plasmas **1**, 1560 (1994)] is studied. The evolution of instabilities can take on several scenarios: a single mode or several modes can be driven unstable at the same time, the spectrum can be steady or pulsating and there can be negligible or anomalous loss associated with the instability. This paper presents a comparison between experimental results and recently developed nonlinear theory. We find many features observed in experiment are compatible with the consequences of the nonlinear theory. Examples include the structure of the saturated pulse that emerges from the onset of instability of a single mode and the decrease but persistence of TAE signals when the applied rf power is reduced or shut off.

[a] Permanent address: A.F. Ioffe Physical-Technical Institute, St. Petersburg 194021, Russia

I. Introduction

The present concept of a tokamak fusion reactor relies on plasma heating by alpha particles produced by the deuterium-tritium reaction. These alpha particles form an energetic ion distribution whose mean speed is comparable to the Alfvén speed, which is much larger than the plasma thermal speed. It has been noted that when energetic particles have speeds comparable to or above the Alfvén speed, they can excite[1,2] shear Alfvén-type waves such as the Toroidal Alfvén Eigenmode (TAE).[3] If these modes grow to large amplitudes, they can eject the fast ions before the ion energy is transferred to the plasma as has been observed under several experimental conditions with either neutral beam or icrf formed energetic particle distributions.[4,5,6] In a fusion reactor such losses would reduce the alpha particle heating efficiency as well as possibly cause local damage to the first wall.[7] Evidence of collective effects induced by alpha particles has recently been observed in TFTR-DT experiments.[8]

The TAE instability threshold has been studied extensively in recent years[9] and it appears that instability in some projected regimes of operation is likely in a reactor plasma. Depending on plasma parameters the TAE instability can have different consequences. Unstable modes may saturate at a low amplitude without causing harm to alpha particle confinement, or be of large enough amplitude to cause rapid global diffusive loss of energetic particles. Therefore, it is important to investigate the saturation mechanisms of these modes.

The basic mechanism for mode saturation arises from the nonlinear behavior of the resonant particle response.[10,11] This response has a general character that is applicable to all systems where instability is due to kinetic resonances. A basic parameter is the characteristic bounce frequency,[10,11] ω_b, of a resonant particle trapped in a finite amplitude electromagnetic wave (quite generally $\omega_b \propto A^{1/2}$ where A is the wave amplitude). In addition the response depends on the rate, ν_{eff}, particles leave and enter the resonance region due to relaxation

processes such as collisions. For example, if ν_s is the 90° pitch angle scattering rate, then $\nu_{\text{eff}} \approx (\omega^2 \nu_s)^{1/3}$ with ω the radian frequency of the mode. Note that ν_{eff} can compete with ω_b even when $\nu_s \ll \omega_b$ since typically $\omega \gg \nu_s$. This competition makes the saturation mechanism more subtle than the commonly used wave trapping concept. It has been shown that for a single mode the value of ω_b at saturation can be expressed in terms of ν_{eff}, γ_L, and γ_d, where γ_L is the linear growth rate due to the kinetic drive in the absence of dissipation in the plasma, and γ_d is the plasma dissipation rate in the absence of the kinetic drive. When saturation is due to a single resonance, the result is generally benign in terms of the particle loss. If there are multiple resonances present, the effect of resonance overlap may greatly increase the fluctuation level, and enhance losses can arise due to global transport.

The purpose of this paper is to establish a framework for interpreting experimental data in terms of the nonlinear response of resonant particles. We present some TFTR measurements of the evolution of the TAE instability driven by energetic particles and we attempt to relate the observations in terms of the recently developed nonlinear theory.

II. Evolution of Instability

A. Single Mode Saturation Near Threshold

There is a variety of data where instability emerges from noise, oscillates somewhat and then approaches a steady state. Such a response is indeed predicted over a range of parameters in the nonlinear theory. We first discuss this case.

We study experiments performed in TFTR with plasmas heated by ICRF fast waves at the cyclotron frequency of the hydrogen minority ions.[8] Unless otherwise specified, the plasma has the following parameters: toroidal magnetic field $B = 3.4$ tesla, plasma major radius $R = 2.62\,\text{m}$, minor radius $a = 0.96\,\text{m}$, plasma current $Ip = 1.3\,\text{MA}$. Helium is the working gas used for breakdown and density feedback control, but there is a substantial

amount (up to 50%) of deuterium ions due to outgas from the carbon limiter. The hydrogen minority ions are heated by $3-10\,\mathrm{MW}$ of 46 MHz fast waves. The heating is anisotropic, with hot tails of trapped particles formed in the region of phase space where banana tips are near the cyclotron resonance. Their energy spread, which increases with rf power is shown in Fig. 1 for a deuterium plasma. These measurements were carried out with a charge exchange technique[12] where Carbon-V is the major electron donor to the escaping protons that have been neutralized by charge exchange. Most of the experimental results discussed here will be for a helium plasma where we expect similar temperature ($0.2-1.0$MeV.) for the H minority species. These energetic ions drive the TAE when they fulfill the resonance condition

$$\Omega_{n,\ell}(\omega) \equiv \omega - n\bar{\omega}_\phi(E, P_\phi, \mu) - \ell\bar{\omega}_\theta(E, P_\phi, \mu) = 0$$

where ω is the mode frequency, $\bar{\omega}_\phi$ is the trapped particle precessional drift frequency and $\bar{\omega}_\theta$ is the poloidal bounce frequency, n the toroidal mode number and l an integer and E, P_ϕ, and μ, are respectively the energy, angular momentum and magnetic moment of resonant particles.

The magnetic oscillations associated with TAE modes are detected by Mirnov coils located near the plasma edge. In some of the plasma shots, internal measurements of local density oscillations associated with TAE modes[8] are carried out with a three channel microwave reflectometer.[13] Some peaks in the frequency spectrum of the reflectometer signal coincide with those in the Mirnov coil data, indicating that these are internal global modes with a significant edge component.

Figure 2 shows the waveforms of the plasma current, line-integrated electron density and the rf power. Observe from Fig. 2 that the rf is turned on at 2.5 sec. to 2.2 MW, a level that does not produce TAE instability in 0.2 sec. as can be seen in Fig. 3. At about 2.7 sec. the level of rf heating is increased to 3.1 MW and the onset of TAE activity is observed

quite soon thereafter as seen in the Mirnov signal output shown in Fig. 3. Thus, as there is no instability observed during the application of the 2.9 MW power level, and instability is observed at an input power level of 3.1 MW, the unstable state is not likely to be more than 10% above the linear stability threshold. Therefore, it is natural to interpret the data on the basis of a theory developed in Ref. 14 for the nonlinear dynamics of a single mode near the instability threshold.

The corresponding equation for the mode amplitude $A(t)$ has the form[14]

$$\frac{dA}{dt} = \gamma A - \frac{\gamma_L}{2} \int_0^{t/2} t'^2 dt' A(t-t') \int_0^{t-2t'} dt'' \exp[-\nu_{\text{eff}}(2t'+t'')]$$

$$\cdot A(t-t'-t'')A(t-2t'-t'') \qquad (1)$$

Apart from a numerical coefficient, which is taken to be unity in this analysis, the absolute value of A is the square of the characteristic nonlinear bounce frequency, ω_b, of a typical resonant particle trapped in the wave. The linear growth rate γ on the right-hand side of Eq. (1) is the difference between the energetic particle contribution, γ_L, and the mode background damping rate γ_d. The theory, which is based on closeness to the instability threshold, assumes that $\gamma = \gamma_L - \gamma_d \ll \gamma_L$.

As the energetic particle distribution formed by the rf heating evolves towards an unstable equilibrium, the growth rate γ changes from negative to positive values. Near the threshold, γ is generally a linear function of time. In order to compare with experiment, we take the growth rate to vary as $\gamma = \sigma t$ (with σ a constant value) over the entire time interval from $t = 0$ (the moment when the system becomes unstable) to the end of the fitted data set. Since γ_L and γ_d nearly balance each other, the time dependence of the equilibrium distribution affects primarily the difference between the two. Otherwise, we will treat γ_L as a constant.

The effective collision frequency, ν_{eff} in Eq. (1) is the rate at which collisional processes renew the distribution function of the resonant particles. In the case of rf heating, ν_{eff} can

be estimated as

$$\nu_{\text{eff}} \approx \chi(\omega^2 \nu_h)^{1/3}, \tag{2}$$

where ν_h is the overall heating rate and χ a numerical coefficient of order unity. This estimate is readily inferred by balancing the mismatch in the resonance condition with the diffusion term of the rf Fokker Planck operator. If we now introduce dimensionless variables $\tau = t\sigma^{1/2}$ and $a \equiv A\gamma_L^{1/2}/\sigma^{5/4}$, Eq. (1) can be rewritten as,

$$\dot{a} = a\tau - \frac{1}{2}\int_0^{\tau/2} d\tau' \tau'^2 a(\tau - \tau') \int_0^{\tau - 2\tau'} d\tau'' \exp[-\nu(2\tau' + \tau'')]$$

$$\cdot\, a(\tau - \tau' - \tau'') a(\tau - 2\tau' - \tau'') \tag{3}$$

with $\nu = \nu_{\text{eff}}/\sigma^{1/2}$.

Equation (3) can be integrated numerically for various values of ν and a_0 (the initial amplitude of a). A set of curves $a(\tau; \nu, a_0)$ are then obtained. These curves define the theoretical signal curve, S_{thr}, given by

$$S_{\text{thr}}(t; k, \sigma, \tau_0, a_0) = k a\left(\tau(t; \tau_0); \nu, a_0\right)$$

with $\tau(t; \tau_0) = \sigma^{1/2}(t - t_1) + \tau_0$ where t_1 is the time of the first exhibited data point. We wish to choose the parameters, $a_0, \tau_0; \sigma, k$ so that $S_{\text{thr}}(t_i)$ is the best fit to the experimental signal at specific times, t_i, shown by the dots in Fig. 4. These points are denoted by $S_{\text{exp}}(t_i)$. We then minimize the expression,

$$\sum_i |S_{\text{exp}}(t_i) - S_{\text{thr}}\left(t_i, k, \sigma, \tau_0, a_0\right)|^2$$

where the summation is over the data points. The best fit values are found to be

$$\nu = 35, \quad \sigma = 5.4 \times 10^4\, s^{-2}, \quad \tau_0 = 5.3,$$

with very little sensitivity to a_0 if it is not too large or too small (this is to be expected to the extent the signal is quasi-stationary depending only on the time dependent growth

rate). The theoretical curve of $\mathcal{A}(\tau)/\nu^2$ is shown by the solid curve in Fig. 4. We can then infer that

$$\nu_{\text{eff}} \equiv \nu\sigma^{1/2} = 8.2 \times 10^3 s^{-1}$$

$$\gamma_L \equiv 10\tau_{\max}\sigma^{1/2} = 1.6 \times 10^4 s^{-1}$$

$$\omega_{b\max} \equiv A_{\max}^{1/2} = \nu\sigma^{5/8}\left(\frac{\mathcal{A}_{\max}}{\nu^2}\right)^{1/2} \Big/ \gamma_L^{1/4} = 8.5 \times 10^3\,\text{rad/s}.$$

The theoretical curve for $\mathcal{A}(\tau)$ exhibits oscillatory behavior and the experimental data also shows an overshoot in the response and an indication of further oscillation. Note that in the theory, the oscillation frequency is not related to the trapping frequency (indeed the theory that is the basis of Eq. (1) assumes that particle trapping does not occur within the time ν_{eff}^{-1}).

We now compare this fit to other independent estimates of the saturation parameters. We find that the theoretical estimate for ω_b, in terms of the perturbed magnetic field, is

$$\omega_b \approx \left(\frac{qnv}{r}\right)\left(\frac{v}{\omega_c}\right)\left(\frac{1}{Rr}\right)^{1/2}\left(\frac{\delta B}{B}\right)^{1/2},$$

From the reflectometer data, an internal level of $\delta B/B \approx 10^{-5}$ is indirectly estimated. Then for $n = 2$, $v = 10^9$cm/s, $r = 30$cm, $q = 1.5$, $B = 3.4$T, and $R = 260$cm, we find $\omega_b = 10^4$ rad/s. This rough estimate for ω_b is consistent with the numerical value obtained with the fitting routine. We now use Eq. (2) to estimate ν_h from the value of ν_{eff} found from our fitting procedure, and we find $\nu_h = 0.5/\chi^3 s^{-1}$. We expect $\nu_h \sim \nu_{\text{drag}} \equiv$ electron energy loss rate which is $\sim 6s^{-1}$ which requires $\chi \sim 0.5$. Thus, given the considerable uncertainty in the choice of the system parameters, we have achieved a consistent correlation between experiment and theory. A more accurate comparison would require more precise spatially resolved experimental data on the distribution function of energetic particles formed during rf heating as well as more information on the mode structure and absolute level of the

magnetic fluctuations. A refined theory can be easily developed for this comparison, where numerical coefficients, which we have taken as unity, are properly evaluated.

B. Multiple Modes Above Threshold

A fine structure in the TAE spectrum also emerges at later time in this run. It usually consists of several peaks that correspond to modes with different frequencies and different toroidal mode numbers. The frequency spectrum is obtained by applying Fourier analysis to the Mirnov coil signal obtained over a time interval Δt. It should be pointed out that the width of the frequency resolution, Δf, is inversely proportional to Δt, i.e. $\Delta f \sim 1/(2\pi\Delta t)$, which is a fundamental limitation. However in our experiment, the slow digitizing rate is a more severe limitation.

Figure 5 shows the TAE spectrum at different times for the run analyzed in Sec. A. Observe that the modes appear in a particular sequence where the lower frequency modes appear first, followed by higher frequency modes. It is generally found that lower frequency modes correspond to higher n modes. In this data set the n-number was determined by analysis of the Doppler shift due to plasma rotation[15] and it was determined that the three modes correspond to $n = 2, 3, 4$. The time sequencing of the different modes reflect the difference in the instability threshold, with new modes appearing as the fast ion distribution builds up in time due to the continuous rf heating.

The resonance condition of all these modes appear to be close to where the radian mode frequency, ω, is comparable to both twice the precessional drift frequency (of a 0.5 Mev particle at $r = 30$cm) and poloidal bounce frequency. Thus the resonance conditions for different modes should be quite spread apart in phase space even for modes oscillating near the same frequency. Theoretically, an independent mode response is then expected as resonances are sufficiently well separated so that the alteration of the distribution function along one resonance, determined by the condition $\Omega_{n,\ell}(\omega) = 0$, does not affect the distribution

along another resonance $\Omega_{n',\ell'}(\omega') = 0$, where $(\omega, \ell, n) \neq (\omega', \ell', n')$.

There is some evidence for this interpretation in the experimental data. In Fig. 6(a) we exhibit raw data from the Mirnov coil signal which exhibits rapid amplitude modulation. The amplitude modulation is caused by the beating of two modes with slightly different frequencies. Fig. 6(b) depicts the frequency spectrum of the signal shown in Fig. 6(a). The two peaks in the spectrum correspond to $n = 2$ and $n = 3$ TAE modes, and the frequency separation equals the amplitude modulation frequency shown in Fig. 6(a), as is expected from the beating of otherwise uncoupled modes. It should also be noted that though the frequency of the two modes are close, $\delta f/f \sim 3\%$, the separation of the resonance conditions is likely to be considerably larger.

By varying the rf power, it is found that the saturated TAE amplitude is approximately proportional to rf power as shown in Fig. 7 and that there are several mode frequencies present at higher rf power. This observation can be compared with theoretical consideration. In this case, if the distribution is steady, and ν_{eff} is large enough, a steady TAE signal is predicted.

The summary of the theoretical saturation predictions is as follows. Near marginal stability, when $\omega_b/\nu_{\text{eff}}$ is small, it follows from Eq. (1) that for a steady wave the energetic particle contribution to the growth rate, γ_{NL}, scales as $\gamma_{NL} \simeq \gamma_L[1 - \alpha(\omega_b/\nu_{\text{eff}})^4]$ with $\alpha \sim 1$. However, when $\omega_b/\nu_{\text{eff}} \gg 1$, it has been determined previously[16] that γ_{NL} scales as $\gamma_{NL} \simeq \gamma_L \nu_{\text{eff}}^3/\omega_b^3$. A simple interpolation formula of these two results, that captures scalings for large and small $\omega_b/\nu_{\text{eff}}$ that is suitable for arbitrary $\nu_{\text{eff}}/\omega_b$, is

$$\gamma_{NL} = \gamma_L \frac{1}{(1 + \omega_b^4/\nu_{\text{eff}}^4)^{3/4}}. \tag{4}$$

The saturated growth rate that can then be inferred from the relation, $\gamma_{NL} - \gamma_d = 0$, is,

$$\omega_b \sim (1 - \gamma_d/\gamma_L)^{1/4}(\nu_h \omega^2 \gamma_L/\gamma_d)^{1/3}. \tag{5}$$

These predicted steady levels have been inferred to be stable[14,16] if,

$$\nu_{\text{eff}} > \gamma_d(1 - \gamma_d/\gamma_L).$$

Note that according to the theoretical formula, the saturation amplitude, $A \sim \omega_b^2$, scales as $\nu_h^{2/3}$. Roughly, we expect the rf diffusion coefficient, which is essentially ν_h, to be proportional to the applied rf power. One also finds that in the experiment the number of modes increases with rf power. These additional modes may explain why the amplitude scales as P_{rf}, rather than $P_{\text{rf}}^{2/3}$, where P_{rf} is the applied rf power. Hence, there appears to be consistency between the experimental observation and theory to achieve increased saturation level with increased rf power.

C. Variations in the Response

Sometimes the response of the nonlinear modes differs from that observed in Sec. B. Consider the run in Fig. 8. In this case the rf power is turned on at 3 sec to 5.8 MW, for 0.17 s. In this section we discuss what happens during this time interval. Notice that this case is somewhat different from the previously analyzed case, in that the first TAE mode to appear is a higher frequency mode, interpreted here as an $n = 4$ mode, followed by lower frequency modes. As the detailed threshold conditions are sensitive to parameters, this may explain the difference from the previously analyzed case. The applied rf power is higher and switched on 0.5 sec. later than the previous case. Thus the plasma may have a slightly different $q(r)$ profile, probably due to more penetration of the current profile. As the thresholds of the three modes are close to each other, the determination of which mode should be unstable first can depend on the detailed profiles. Also note that the later appearing modes are detected with a stronger Mirnov signal. This could be if the higher n-modes are more internally localized than lower n-modes, and then they would be difficult to detect. Thus the magnitude of the different signals should not reflect the relative strength

between the different modes.

We see from Fig. 8(b) and from Fig. 9(a), that the highest frequency $n = 4$ mode rises to a steady level until the next lower frequency mode (the $n = 2$ mode) appears at $t = 3.076\,\text{sec}$. From Fig. 9(b) we observe that this mode then rises to a near steady level, until the appearance of the next lower frequency mode ($n = 2$). On the other hand, from Fig. 8(a), we see that first mode response is sometimes quenched during the rising phase of the second mode. At 3.087 sec. a third mode appears, and rises to an oscillatory, rather than a steady level. During the time when all three modes are excited, they all appear to be oscillating.

It may be possible to interpret the behavior just described within the framework of the theoretical picture that we have formulated. In particular the $n = 2$ mode, which seems closer to threshold than the other two, allows finding a good fit, similar to that described in Sec. A. Note that a steady response is to be expected for a single mode only if ν_h is sufficiently large; otherwise oscillations are expected, which can perhaps explain the oscillations in Fig. 8b and in more detail in Fig. 9.

In addition other factors may come in that are beyond the scope of the independent mode theory we have developed. Some examples include: 1) Modes do not oscillate independently because of the overlap in the resonance response. The assumption of independent modes fails if $\nu_{\text{eff}} > \Delta\Omega$, where $\Delta\Omega$ is the separation between resonances. Analysis of what happens in this case has not as yet been developed, but it is plausible to expect this effect to couple the otherwise independent modes and to induce additional oscillations of the mode amplitude. For example oscillations could arise if the excitation of one mode depletes the drive for another mode.

Another possibility is that there is mode overlap, that arises when $\omega_b > \Delta\Omega$. A mode overlap situation is difficult to sustain in steady state, but it leads to substantially higher

saturation levels than the independent mode case. As the amplitudes for the modes shown in Fig. 8 are similar to the mode amplitudes shown Fig. 3, mode overlap as an explanation of the oscillations seen in Figs. 8 and 9 is not likely.

One might invoke fluid mode coupling, proportional to $(\delta B/B)^2$ as a cause of the oscillations. We do not think that this mechanism is competitive in our case since the mode amplitudes are still small. $\delta B/B \sim 10^{-5} - 10^{-4}$ so that such a nonlinear effect is likely to be insignificant.

In summary, it is quite likely that a more careful analysis of our basic nonlinear picture can explain the saturation levels observed in Figs. 8 and 9. However, to obtain a quantitative comparison of theory and experiment, both more careful theoretical calculations need to be performed and more precise experimental measurements are required.

D. Persistence of Instability After rf Power Reduction

A feature of several pieces of data, is that TAE activity persists even after the rf power is turned down to a level that can not support a stable mode in steady state or when the rf power is turned off completely. This persistence is important evidence in support of the picture we have of how saturation is determined.

In the run described in Sec. C the rf is suddenly turned down at 3.17 sec., in a fraction of a msec., from 5.8 MW to 3.5 MW. The TAE modes stay in the plasma for more than 10 ms and only then disappears. Thus the 3.5 MW power level does not sustain a distribution function that is unstable to the TAE mode. Clearly it takes some time for the distribution function to relax to a stable state. However, the instability level does not immediately have a large change when the power level is lowered. Figure 10(a) shows the fully developed instability spectrum before the rf power decrease and Fig. 10(b) shows TAE spectrum immediately after the rf power decrease. Note that the $n = 3$ mode still has an amplitude at a level comparable to the previous level. The $n = 2$ mode is reduced in amplitude, while the first

mode is being observed in a phase that it is at a low level. We note that the theory predicts that for the same distribution function, that a steady state amplitude scales as $\nu_h^{2/3}$, and we expect ν_h to be proportional to P_{rf}, with P_{rf} the rf power level being applied. Thus a 60% decrease in rf power predicts a rapid decrease to about 0.7 of the original TAE amplitude immediately after the rf power is lowered. The time scale of this transition is roughly ν_{eff}. These inferences are consistent with experimental observation. We further note that the $n = 2$ mode is the first to disappear later in time. This is consistent with the observation that it was the last to go unstable. The slowing down time of 0.5 Mev hydrogen ions in the plasma with 5 kev electron temperature and a density of $3 \times 10^{13}\text{cm}^{-3}$ is about 300 ms. Thus the mode decay is still appreciably shorter than the slowing down time of fast ions. This can be understood if the instability is close to threshold, so that the decreasing population of the hydrogen distribution in the resonance region causes the mode to stabilize in a small fraction of a slowing down time.

If there is no rf power to diffuse energetic particles in velocity space, the TAE amplitude can fall rapidly, to either a lower level or be turned off completely. These two possibilities are experimentally depicted in Fig. 11, which show the decay of TAE modes after the rf power is purposely completely switched off (within 0.5 ms.). Figure 11(a) is for a 1.8 MA deuterium plasma at 4.5 tesla magnetic field with 20 MW of deuterium neutral beam heating. The ICRF power was about 5.5 MW and 63 Mhz, near the instability threshold. In this case the TAE modes disappear within 1 ms after the rf power is switched off. Figure 11(b) shows the results for a plasma with similar parameters and rf heating, but with the addition of a 15 MW of neutral tritium beam power which produces 3 MW of fusion power, so that there is an alpha particle component that is another drive for TAE modes. The drive of the instability is stronger because of the fast alpha particles in the plasma. Low amplitude TAE modes last 15 ms after the rf is switched off.

The above results fit into the nonlinear description as follows. In Fig. 11(a) the rf power is

enough to produce instability just above the threshold. When the rf is turned off completely, there still remains a diffusion mechanism due to pitch angle scattering, ν_s, which is much less than ν_h (recall ν_h is the heating rate with rf). It is possible for this diffusion mechanism to temporarily maintain an unstable distribution with a lower TAE amplitude after a time, ν_{eff}, where now $\nu_{\text{eff}} \simeq (\nu_s \omega^2)^{1/3}$ which is reduced from the case with rf present. At the same time the weight of the distribution function at resonance is being reduced by the electron drag. For this data, the result is a rapid decay of the TAE noise as observed in Fig. 11(a) without an apparent lower-level persistence of the mode.

When an appreciable drive comes from the alpha particles, (it is estimated that $\gamma_{L\alpha} \sim (0.1 - 0.3)\gamma_{Lp}$ where $\gamma_{L\alpha}$ is the linear drive from alpha particles and γ_{Lp} the linear drive from protons) we see in Fig. 11(b) that a nearly steady amplitude of TAE noise is established at apparently three times the level of Fig. 11(a). (It is not totally clear that the different relative amplitudes in Figs. 11(a) and 11(b) can be calibrated with respect to each other, as the internal mode structure of the two modes can be different, since the observed frequencies are different.) Before the rf turn-off the steady state level is determined by a weighted average of the diffusive processes on the alpha particles and the rf heated trapped particles. Now, $\gamma_L = \gamma_{L\alpha} + \gamma_{Lp}$, is the TAE growth rate (in absence of background damping) due to the alpha particle and rf heated particles respectively. With alpha particles the system should be further above the instability threshold than in the case without alpha particles. The steady state instability level can be determined from a straightforward generalization of the saturation theory near marginal stability. Now we have two species contributing to instability. One is the resonant protons, whose effective collision frequency, $\nu_{\text{eff}p}$, is

$$\nu_{\text{eff}p1} \simeq (\omega^2 \nu_{hp})^{1/3}, \text{ with rf turned on,}$$

$$\nu_{\text{eff}p2} \simeq (\omega^2 \nu_{sp})^{1/3}, \text{ with rf turned off,}$$

where ν_{sp} is the 90° scattering rate of the proton, which is much less than ν_{hp}. The other

drive is the alpha particle, whose effective collision frequency, $\nu_{\mathrm{eff}\alpha}$, is

$$\nu_{\mathrm{eff}\alpha 1} \simeq (\omega^2 \nu_{h\alpha})^{1/3}, \text{ with rf turned on}$$

$$\nu_{\mathrm{eff}\alpha 2} \simeq (\omega^2 \nu_{s\alpha})^{1/3}, \text{ with rf turned off}$$

with $\nu_{s\alpha}$ the 90° alpha particle scattering rate ($\nu_{s\alpha} \sim \nu_{sp}(E_p/E_\alpha)^{3/2}$ with E_α and E_p the mean energies of alphas and protons). Now using Eq. (4) for each species, the structure of the stability formula that determines saturation with two species is,

$$\gamma_{Lp}\left[\frac{1}{1+(\omega_{bp}/\nu_{\mathrm{eff}p})^4}\right]^{3/4} + \gamma_{L\alpha}\left[\frac{1}{1+(\omega_{b\alpha}/\nu_{\mathrm{eff}\alpha})^4}\right]^{3/4} = \gamma_d. \tag{6}$$

We now assume that $\lambda = (\omega_{b\alpha}/\omega_{bp})(\nu_{\mathrm{eff}p}/\nu_{\mathrm{eff}\alpha}) \gg 1$. This seems to be a very good approximation. In other unpublished calculations we find that $\omega_{b\alpha}/\omega_{bp} \approx 10$ for parameters applicable to the TFTR experiment, where $\omega_{b\alpha}$ are for toroidally passing alpha particles whose energy is $\sim 3\,\mathrm{MeV}$, while the resonant protons have an energy less than 1 MeV. One also has $\nu_{\mathrm{eff}\alpha} < \nu_{\mathrm{eff}p}$. For example, when the rf is turned off $\nu_{\mathrm{eff}\alpha}/\nu_{\mathrm{eff}p} \approx (E_p/E_\alpha)^{1/2}$, where E_α and E_p are the energy of the resonant alpha particles and protons. Similarly, when the rf is turned on, we should have $\nu_{\mathrm{eff}p} > \nu_{\mathrm{eff}\alpha}$, as the energetic protons, which are toroidally trapped and turn near the cyclotron frequency, interact more efficiently with the rf, than the alpha particles, which for the most part are passing rapidly through the second harmonic cyclotron resonance. The result is that $\lambda \gtrsim 25$ should typically be satisfied for TFTR parameters.

The solution to Eq. (6) is obtained assuming $\gamma_{Lp} \gg (\gamma_{Lp} - \gamma_d), \gamma_{L\alpha}$. Hence, in Eq. (6) the proton term can be replaced by $\gamma_{Lp}[1-(\omega_{bp}/\nu_{\mathrm{eff}p})^4]$. However, because λ is large, one usually finds that $\omega_{b\alpha}/\nu_{\mathrm{eff}\alpha}$ will be large. Hence in Eq. (6), the alpha term is $\gamma_{L\alpha}\nu_{\mathrm{eff}p}^3/(\lambda^3\omega_{bp}^3)$. We then solve by interpolation and the saturated level for sufficiently large λ is found to be,

$$\frac{\omega_{bp}}{\nu_{\mathrm{eff}p}} \approx \left[1 - \frac{\gamma_d}{\gamma_{Lp}} + \left(\frac{\gamma_{L\alpha}}{\lambda^3\gamma_{Lp}}\right)^{4/7}\right]^{1/4}, \quad \text{if} \quad \frac{\gamma_d}{\gamma_{Lp}} < 1 \tag{7a}$$

$$\frac{\omega_{pb}}{\nu_{effp}} \approx \frac{1}{\lambda}\left[\left(\frac{\gamma_{L\alpha}}{\gamma_d - \gamma_{Lp}}\right)^{4/3} - 1\right]^{1/4}, \quad \text{if} \quad \frac{\gamma_d}{\gamma_{Lp}} > 1 > \frac{\gamma_d}{\gamma_{Lp} + \gamma_{L\alpha}}. \tag{7b}$$

Note that Eq. (7a) implies, that for large λ, the saturation level ω_{pb} will be insensitive to $\gamma_{L\alpha}$ unless $1 - \gamma_d/\gamma_{Lp}$ is extremely small.

Now when the rf is turned off, the system is sufficiently above marginal stability that the reduction of the drive due to drag is not fast enough to stabilize the system, and the system reaches its new steady level, for which the amplitude is a factor $(\nu_{sp}/\nu_{h\alpha})^{2/3}$ of the original one. Note that for $Z_{\text{eff}} \simeq 2$, that $\nu_{sp} \approx 0.7\, s^{-1}$ is appropriate for 500 keV protons and $\nu_{hp} \approx 6.0\, s^{-1}$ is an estimate for the proton heating rate. We then find that $(\nu_{sp}/\nu_{hp})^{2/3} \sim 4.2$, which is comparable to the decrease in the TAE amplitudes observed in Fig. 11 just after the rf is turned off. This TAE signal persists for 15 ms., whereupon the drag causes overall stabilization of the system. It should be pointed out that alpha particles are not necessary for the above phenomenon when the rf power is high enough so that the TAE mode is substantially above the instability threshold. Theory then predicts that TAE modes will persist after rf turn-off. TAE modes driven by energetic protons have indeed been found in other data to persist after the rf is turned off.

E. Particle Loss Induced by TAE Instability

When the instability is driven to large enough amplitudes, mode overlap is expected to occur. The resonant particles can then diffuse unhindered over the regions of phase space where there are particle-wave resonances, that may include the plasma boundaries. Theoretical studies have also established that the mode amplitudes, arising from resonance overlap from several modes (say N modes), are substantially larger than when there are N-nonoverlapped modes. With overlap, the wave energy release typically scales as $WE \sim N^2$, where WE is the wave energy release of N independent nonoverlapped modes. Frequently the instantaneous loss rate is so rapid, that the sources and sinks cannot sustain a steady state,

and pulsation relaxation occurs,.i.e, the instability exhibits a bursting behavior. Pulsations have been observed in TFTR that appear consistent with this picture.

For neutral beam driven TAE modes, the instantaneous fast ion loss rate induced by the instability is higher than the neutral beam fueling rate. Therefore, the instability exhibits bursting behavior as shown in Fig. 12. TAE modes grow to a large amplitude, much higher than the noise level. The mode frequency can be determined from the raw data directly without going through Fourier analysis, and the growth rate can also be estimated from the raw data. Fast deuterium ions were ejected rapidly as inferred from the reduction of the neutron emission rate, and then the modes become stable. Neutral beam fueling continues during the quiescent period and restores the fast ion pressure gradient so that the instability repeats itself. This process clamps the fast ion population near the instability threshold. The quiescent period gets longer at lower neutral beam power as expected. The TAE damping rate in this plasma is calculated to be $\gamma_d/\omega \sim 1\%$, and the growth rate from raw data is estimated to be $\gamma/\omega \sim 0.7\%$. Therefore, the driving term is $\gamma_L/\omega \sim 1.7\%$. The density oscillation δn associated with TAE modes driven by neutral beams can be detected by beam emission spectroscopy. It is related to the plasma displacement through the density gradient: $\delta n = -\boldsymbol{\xi} \cdot \boldsymbol{\nabla} n$. From the plasma displacement, we can stimate the magnetic field associated with the TAE mode from the relation $\delta \mathbf{B} = \boldsymbol{\nabla} \times (\boldsymbol{\xi} \times \mathbf{B})$. For this experiment, we obtain $\delta B/B \sim 10^{-3}$. This quantity is at least one order of magnitude larger than the maximum TAE amplitude driven by hot ions produced by ICRF heating. Because of the low plasma current and low magnetic field in this experiment, the energetic ions have large orbits. It is possible for a passing ion to move into a barely trapped orbit due to interaction with TAE modes, and the banana orbit is large enough to escape from the plasma. However, previous computer simulations[7] indicates that we cannot account for the high (5-10%) energetic ion loss rate shown in Fig. 12, if there is only one TAE mode in the plasma at the level estimated here. Note however, that the TAE bursts shown in Fig. 12, show several mode frequencies.

Though the fequency of the three small bursts at 3.694 s, 3.697 s and 3.699 s have one dominant peak, there are also additional peaks that are one half to one third weaker than the dominant peak in the frequency spectrum. These additional modes could account for the particle loss. For the bursts at 3.690 s and 3.701 s, there are two peaks of comparable magnitude, and the corresponding drop in neutron rate is more than twice larger, indicating an even more efficient diffusion mechanism. Although the variation of coupling strength between different TAE modes and the Mirnov coil is not known, the data indicates that instability is leading to resonance overlap which plays an important role in the loss process that limits the number of energetic ions that can be stored in the plasma.

In ICRF experiments, TAE bursts are rare but they have also been observed. Figure 13 depicts the raw data from the Mirnov coil signal which shows the sudden increase of mode amplitude. The frequency spectrum hardly changes before, during and after the burst. It is found that the burst coincides with a sawtooth crash in the plasma. Figure 14 depicts the bursts of TAE modes and sawtooth activity observed in the soft x-ray emission from the plasma core. There is excellent correlation between these events.

Possible explanations are as follows. The first is that there is a transient increase in the linear drive due to (a) the sudden change in the energetic particle population of the sawtooth crash arising from movement of these particles from the $q = 1$ surface to larger q-values; (b) a possible transient decrease of the TAE damping mechanism arising from the change of electron temperature associated with a sawtooth crash. A second possibility is that the combination of the perturbed magnetic fields associated with the sawtooth and the multiple TAE modes, increase the domain of orbit stochasticity, leading to enhanced loss. Further work is needed to clarify this loss phenomenon.

III. Discussion

In this paper, we presented experimental data on the evolution of TAE instability in TFTR plasmas. We have been able to show that a wide variety of experimental responses are compatible with an analytic nonlinear picture that has recently been developed. The experimental evolution of the TAE amplitude at the onset of instability is fitted to analytic theory and the saturation levels and relaxation rates predicted by fits are compatible with experimental conditions. The rapid decay, but the continued persistence for about 15 msec. at a lower level of TAE modes after the rf is switched off, is also explained. Discussion was given of why one should have pulsation or steady TAE levels, and why with larger linear drives, particle loss due to mode overlap can arise.

Though we have encouraging correlation between experimental data and the nonlinear theory, our understanding is far from complete. Several of our interpretations need further scrutiny with additional data. We explained the disappearance of the TAE mode in Fig. 10a after the rf was turned off as arising from the reduction of the drive in a system that was very close to marginal stability. It is plausible that the reduction of the drive in the vicinity of resonance arising from drag and pitch angle scattering of the overall narrow distribution can suppress the instability faster than the distribution function in the immediate vicinity of the resonance can relax towards an unstable shape through the relatively rapid [on the time scale of $(\nu_s\omega^2)^{-1/3}$] scattering process. In other experimental situations, the rf heating prepares a system further above marginal stability, so that upon rf turn-off, the TAE mode decreases, but then persists at a lower level, for some fraction of a slowing down time. One should also observe cases where the TAE modes persists after turn-off for substantially more than the $\sim 1/20$ of a slowing down time we have observed in the data set analyzed in this paper.

It is interesting to point out that it should also be possible to see an increase of the TAE

amplitude after rf turn-off. The nonlinear theory predicts a steady level for the TAE mode given by $\omega_b \sim \nu_{\text{eff}}(1-\gamma_d/\gamma_L)^{1/4}$ only if ν_{eff} is greater or of order γ_L/γ_d. However, if ν_{eff} is less than or $\gamma_L - \gamma_d$, an explosive instability of the nonlinear state is predicted[15] that gives rise to an excited pulse that reaches a level ω_b which is of order γ_L. Clearly this level can be larger than the level the TAE mode achieves when the rf is on.

Equation (7) has the interesting consequence when the proton drive is slightly destabilizing and when there is an additional alpha particle drive, $\gamma_{L\alpha}$. It indicates that the saturation level, ω_{bp}, can be insensitive to $\gamma_{L\alpha}$ unless the proton drive is just enough to bring the TAE instability near the threshold. In rf DT experiments,[8] which have additional alpha particle drive, it is observed that the TAE amplitude was higher than in similar DD plasmas. An apparent interpretation is that this is the direct consequence of having the alpha drive in addition to the drive from the rf heated protons. However, for such an explanation to be compatible with theory, it is required that γ_{Lp} not exceed γ_d by more than a $\frac{1}{2}\%$ or so. In the data published in Fig. 2 of Ref. 8 the TAE amplitude is very low in the DD shots and it is indeed possible that $\gamma_{Lp} - \gamma_d \lesssim .005\gamma_{Lp}$, thereby allowing the saturation level in DT to be enhanced by the alpha component. However, we should also point out that even with the same rf power, $\gamma_{Lp} - \gamma_d$ may not exactly be the same in the DT and DD plasmas. A slightly higher value of $\gamma_{Lp} - \gamma_d$ in DT plasmas can contribute to the observed difference in the TAE amplitude, compared to the rf heated DD plasma, without alpha particles directly causing significant saturation enhancement. It requires precise knowledge of γ_{Lp} and γ_d to resolve these mechanisms.

A major problem preventing us from more detailed analysis is the lack of information on the evolution of the fast ion distribution function $f(\mathbf{r}, \mathbf{v}, t)$. The diagnostics providing this information is not sufficiently developed to determine $f(\mathbf{r}, \mathbf{v}, t)$ with good enough spatial, temporal and velocity space resolution. However, we still have managed to relate our data to certain features of nonlinear physics. More analysis will be needed to verify, with addi-

tional experimental data, that there is overall consistency of the interpretations and fitting parameters given here. If the method we have developed is confirmed by future analysis of other experimental data, this method may become the basis of a diagnostic procedure that will give new information about $f(\mathbf{r}, \mathbf{v}, t)$ and understanding of energetic particle dynamics that is an essential aspect of tokamak operation in fusion relevant regimes.

Acknowledgments

We are appreciative of useful discussions with K. McGuire, E. Fredrickson, R. Nazikian, S. Zweben, and G.Y Fu. One of us (HLB) would like to thank the Princeton Plasma Physics Laboratory for hosting a visit to complete this work.

This work is supported by the U.S. Department of Energy, Contract Nos. DE-AC02-76-CH0-3073 and DE-FG03-96ER-54346.

References

1. M.N. Rosenbluth and P.H. Rutherford, Phys. Rev. Lett. **34**, 1428 (1975).

2. G.Y. Fu and J.W. Van Dam, Phys. Fluids B **1** 1949 (1989).

3. C.Z. Cheng, Liu Chen, and M.S. Chance, Ann. Phys. (N.Y.) **161**, 21 (1985).

4. K.L. Wong R.J. Fonck, S.F. Paul, D.R. Roberts, E.D. Fredrickson, R. Nazikian, H.K. Park, M. Bell, N.L. Bretz, R. Budny, S. Cohen, G.W. Hammett, F.C. Jobes, D.M. Meade, S.S. Medley, D. Mueller, Y. Nagayama, D.K. Owens, and E.J. Synakowski, Phys. Rev. Lett. **66**, 1874 (1991).

5. W.W. Heidbrink, E.J. Strait, E. Doyle, and R. Snider, Nucl. Fusion **31**, 1635 (1991).

6. R.J. Hawryluk, H. Adler, P. Alling, C. Ancher, H. Anderson, J.L. Anderson, D. Ashcroft, Cris W. Barnes, G. Barnes, S. Batha, M.G. Bell, R. Bell, M. Bitter, W. Blanchard, N.L. Bretz, R. Budny, C.E. Bush, R. Camp, M. Caorlin, S. Cauffman, Z. Chang, C.Z. Cheng, J. Collins, G. Coward, D.S. Darrow, J. DeLooper, H. Duong, L. Dudek, R. Durst, P.C. Efthimion, D. Ernst, R. Fisher, R.J. Fonck, E. Fredrickson, N. Fromm, G.Y. Fu, H.P. Furth, C. Gentile, N. Gorelenkov, B. Grek, L.R. Grisham, G. Hammett, G.R. Hanson, W. Heidbrink, H.W. Herrmann, K.W. Hill, J. Hosea, H. Hsuan, A. Janos, D.L. Jassby, F.C. Jobes, D.W. Johnson, L.C. Johnson, J. Kamperschroer, H. Kugel, N.T. Lam, P.H. LaMarche, M.J. Loughlin, B. LeBlanc, M. Leonard, F.M. Levinton, J. Machuzak, D.K. Mansfield, A. Martin, E. Mazzucato, R. Majeski, E. Marmar, J. McChesney, B. McCormack, D.C. McCune, K.M. McGuire, G. McKee, D.M. Meade, S.S. Medley, D.R. Mikkelsen, D. Mueller, M. Murakami, A. Nagy, R. Nazikian, R. Newman, T. Nishitani, M. Norris, T. O'Connor, M. Oldaker, M. Osakabe, D.K. Owens, H. Park, W. Park, S.F. Paul, G. Pearson, E. Perry, M. Petrov, C.K. Phillips, S. Pitcher, A. Ramsey, D.A. Rasmussen, M.H. Redi, D. Roberts, J. Rogers, R. Rossmassler, A.L. Roquemore, E. Ruskov, S.A. Sabbagh, M. Sasao, G. Schilling, J. Schivell, G.L. Schmidt, S.D. Scott, R. Sissingh, C.H. Skinner, J. Snipes, J. Stevens, T. Stevenson, B.C. Stratton, J.D. Strachan, E. Synakowski, W. Tang, G. Taylor, J.L.

Terry, M.E. Thompson, M. Tuszewski, C. Vannoy, A. von Halle, S. von Goeler, D. Voorhees, R.T. Walters, R. Wieland, J.B. Wilgen, M. Williams, J.R. Wilson, K.L. Wong, G.A. Wurden, M. Yamada, K.M. Young, M.C. Zarnstorff, and S.J. Zweben, Phys. Plasmas **1**, 1560 (1994).

7. D.J. Sigmar, C.T. Hsu, R. White and C.Z. Cheng, Phys. Fluids B **4**, 1506 (1992).

8. K.L. Wong, G.L. Schmidt, S.H. Batha, R. Bell, Z. Chang, L. Chen, D.S. Darrow, H.H. Duong, G.Y. Fu, G.W. Hammett, F. Levinton, R. Majeski, E. Mazzucato, R. Nazikian, D.K. Owens, M. Petrov, J.H. Rogers, G. Schilling, and J.R. Wilson, Phys. Rev. Lett. **76**, 2286 (1996).

9. G.Y. Fu, C.Z. Cheng, and K.L. Wong, Phys. Fluids B **5**, 4040 (1993).

10. B.N. Breizman, H.L. Berk, and H. Ye, Phys. Fluids B **5**, 317 (1992).

11. H.L. Berk, B.N. Breizman, F. Fitzpatrick, M.S. Pekker, H. Vernon Wong, and K.L. Wong, Phys. Plasmas **3**, 1827 (1996).

12. M.P. Petrov, V.I. Afanasyev, C. Corti, *et al.*, 19th EPS Conference, Innsbruck, 1992, report 6–2, I 103.

13. E. Mazzucato and R. Nazikian, Phys. Rev. Lett. **71**, 1840 (1993).

14. H.L. Berk, B.N. Breizman, and M. Pekker, Phys. Rev. Lett. **76**, 1256 (1996).

15. K.L. Wong, J.R. Wilson, Z.Y. Chang, G.Y. Fu, E. Fredrickson, G.W. Hammett, C. Bush, J. Snipes, and G. Taylor, Plasma Phys. Contr. Fusion **36**, 879 (1994).

16. H.L. Berk and B.N. Breizman, Phys. Fluids B **2**, 2246 (1990).

FIGURE CAPTIONS

FIG. 1. Variation of the effective temperature of the hydrogen minority ions vs. applied rf power in deuterium plasmas.

FIG. 2. Wave forms showing time history of plasma current, line-integrated electron density and applied rf power.

FIG. 3. Evolution of the TAE amplitude detected by a Mirnov coil at the plasma edge.

FIG. 4. Growth of $n = 2$ TAE mode amplitude showing oscillations near saturation level. Only one mode present during this time interval.

FIG. 5. Frequency spectrum of Mirnov signal at different times of discharge.

FIG. 6. Mirnov coil signal showing the amplitude modulation resulting from beating of two modes with slightly different frequencies.

FIG. 7. Variation of TAE amplitude with applied rf power.

FIG. 8. (a) rf power wave form; (b) 3-D plot showing evolution of frequency spectrum of the Mirnov coil signal; (c) Frequency spectrum at 3.092 sec.

FIG. 9. Evolution of mode amplitudes for the three modes shown in Fig. 8.

FIG. 10. Frequency spectrum (a) just before and (b) just after the rf power is reduced from 5.8 MW to 3.5 MW.

FIG. 11. Decay of TAE mode after the rf power is completely turned off. (a) Deuterium plasma; (b) Deuterium-tritium plasma.

FIG. 12. Correlation between the variation of neutron flux and the TAE amplitude indicating energetic ion loss induced by TAE modes.

FIG. 13. Bursting behavior of TAE modes excited by energetic ions in ICRF H-minority heated plasma.

FIG. 14. Correlation between (a) sawteeth activities and (b) TAE bursts.

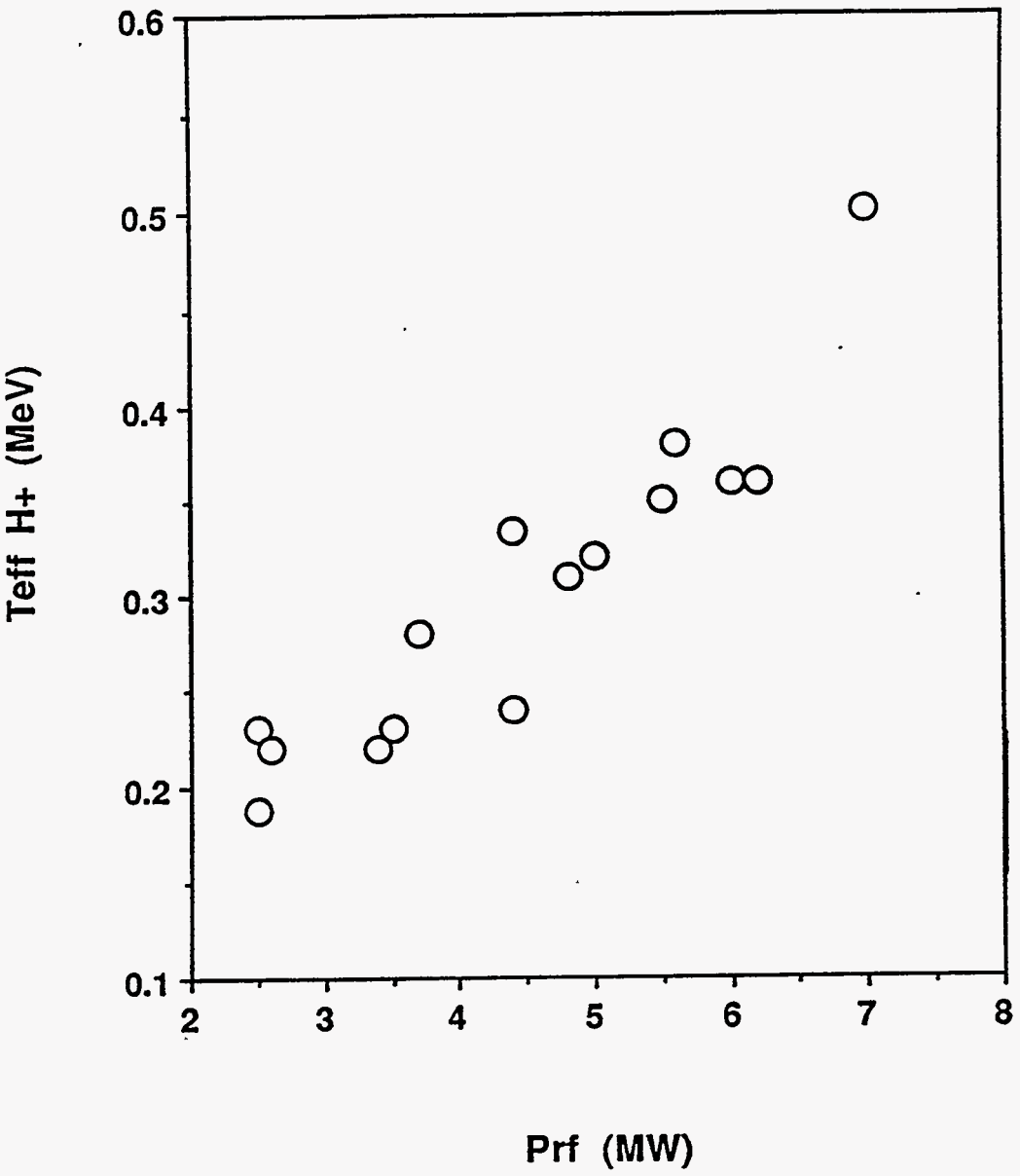

Fig. 1

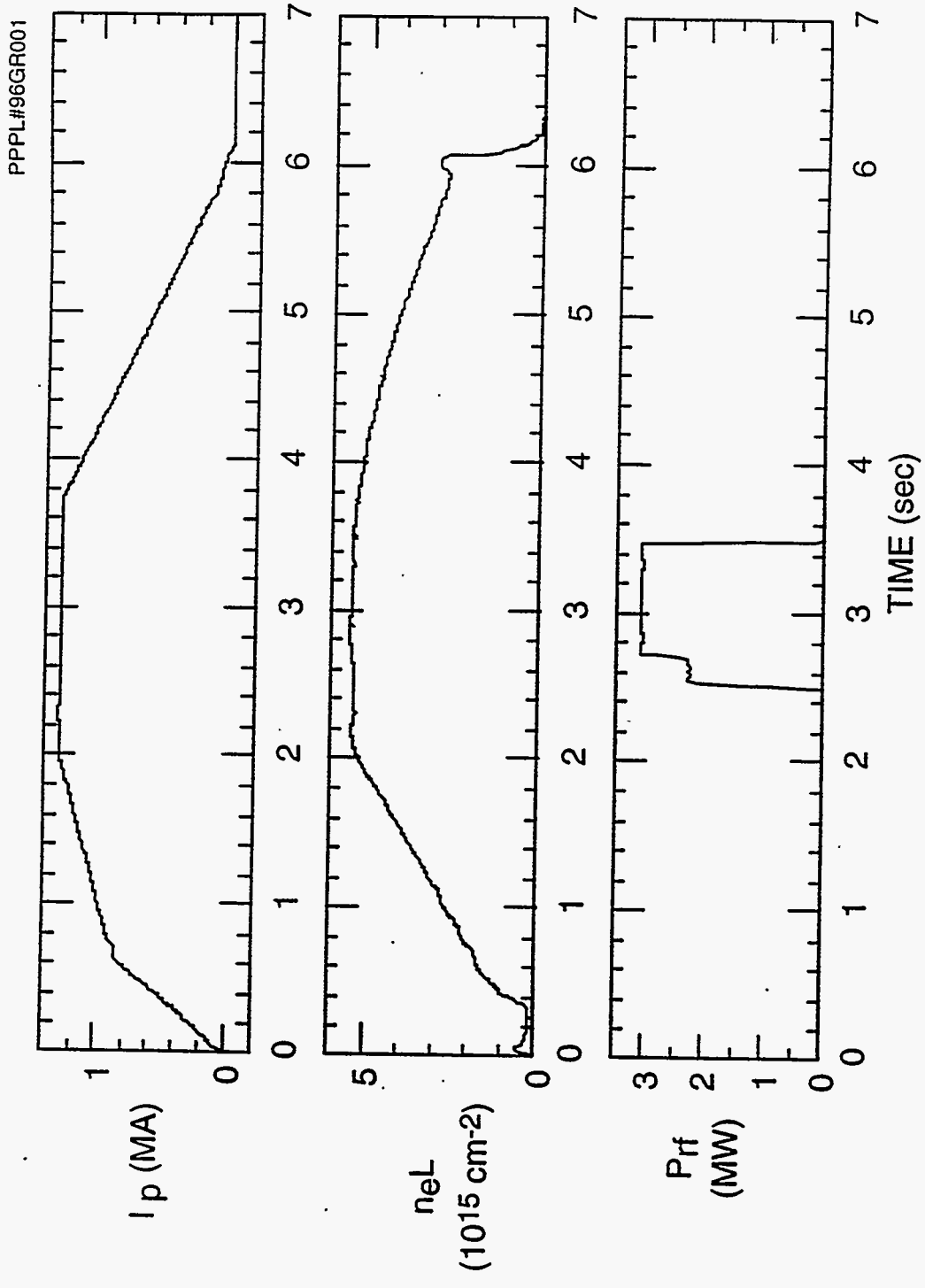

Fig. 2

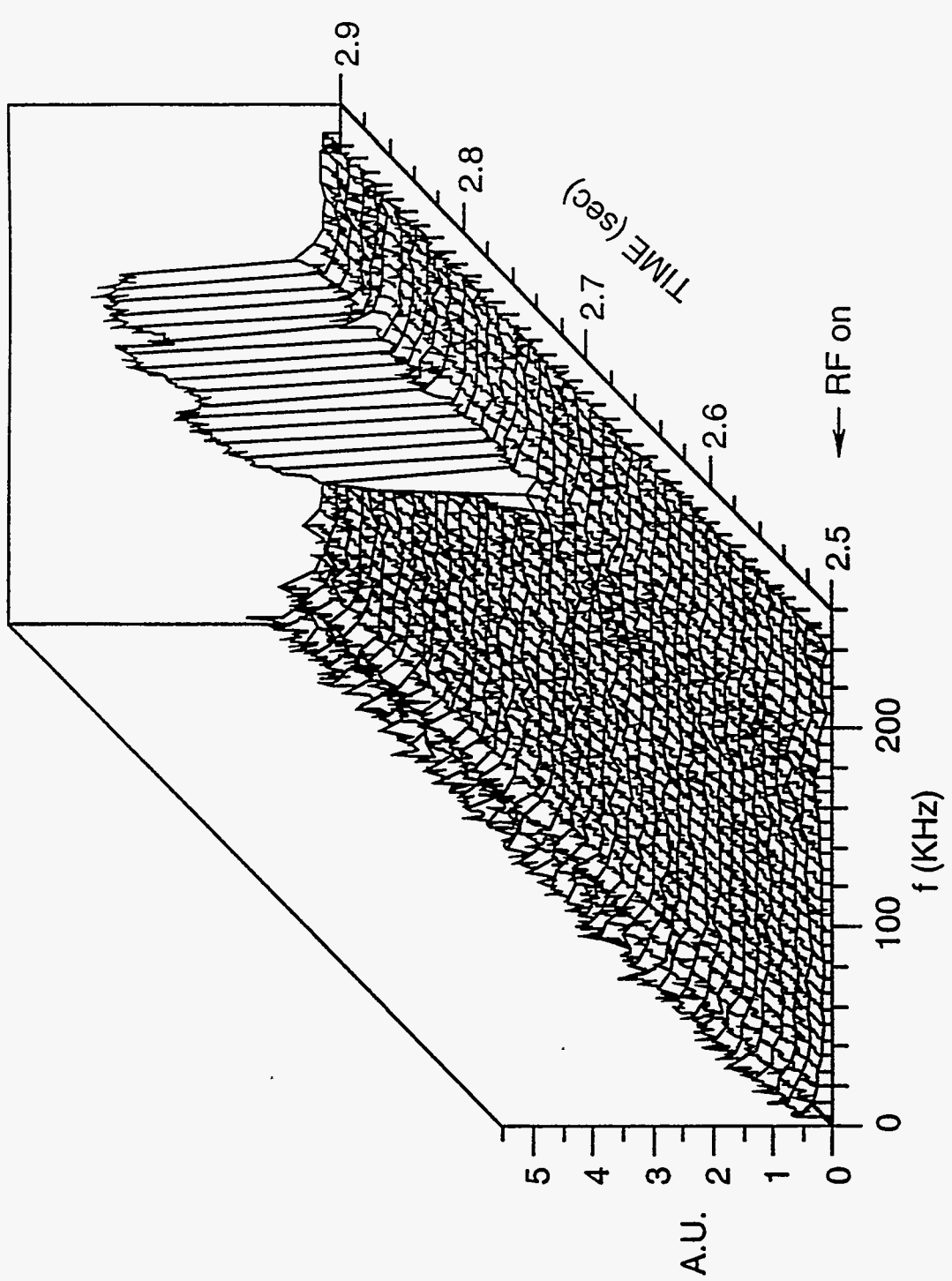
PPPL#96GR002
2.9
2.8
2.7
2.6
2.5
TIME (sec)
RF on
0
100
200
f (KHz)
0
1
2
3
4
5
A.U.

Fig. 3

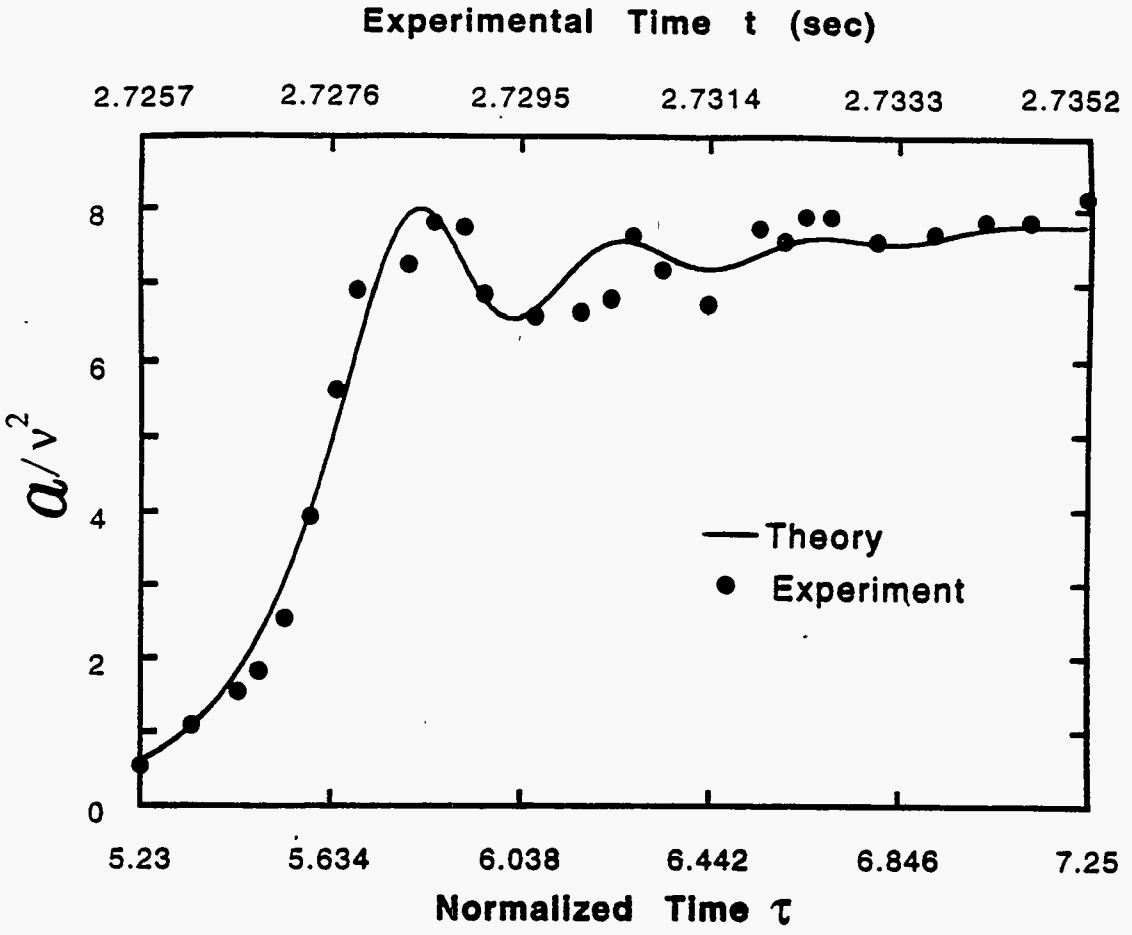
Experimental Time t (sec)
2.7257
2.7276
2.7295
2.7314
2.7333
2.7352
8
6
4
2
0
a/v^2
Theory
Experiment
5.23
5.634
6.038
6.442
6.846
7.25
Normalized Time τ

Fig. 4

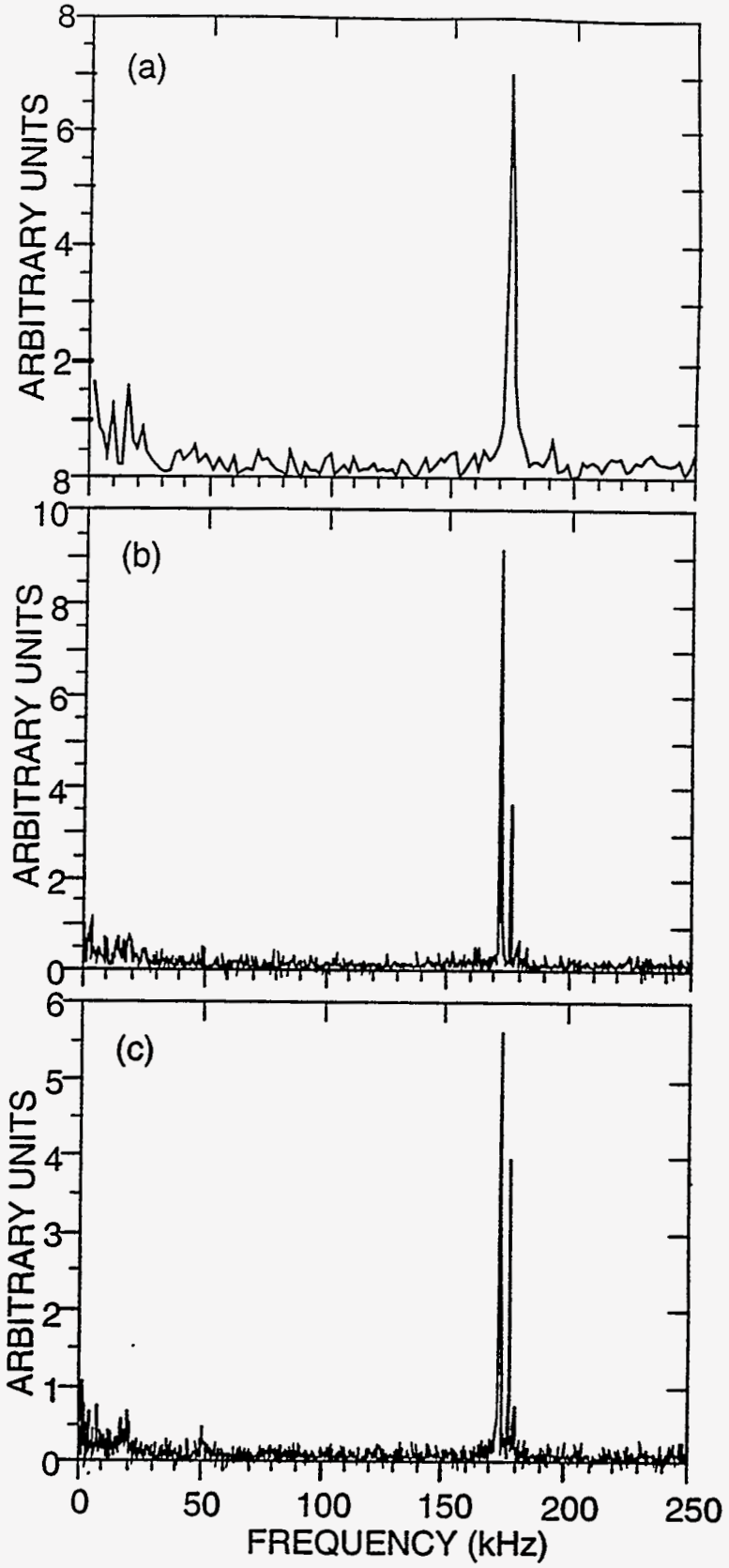
(a)
(b)
(c)
ARBITRARY UNITS
ARBITRARY UNITS
ARBITRARY UNITS
FREQUENCY (kHz)
0
50
100
150
200
250

Fig. 5

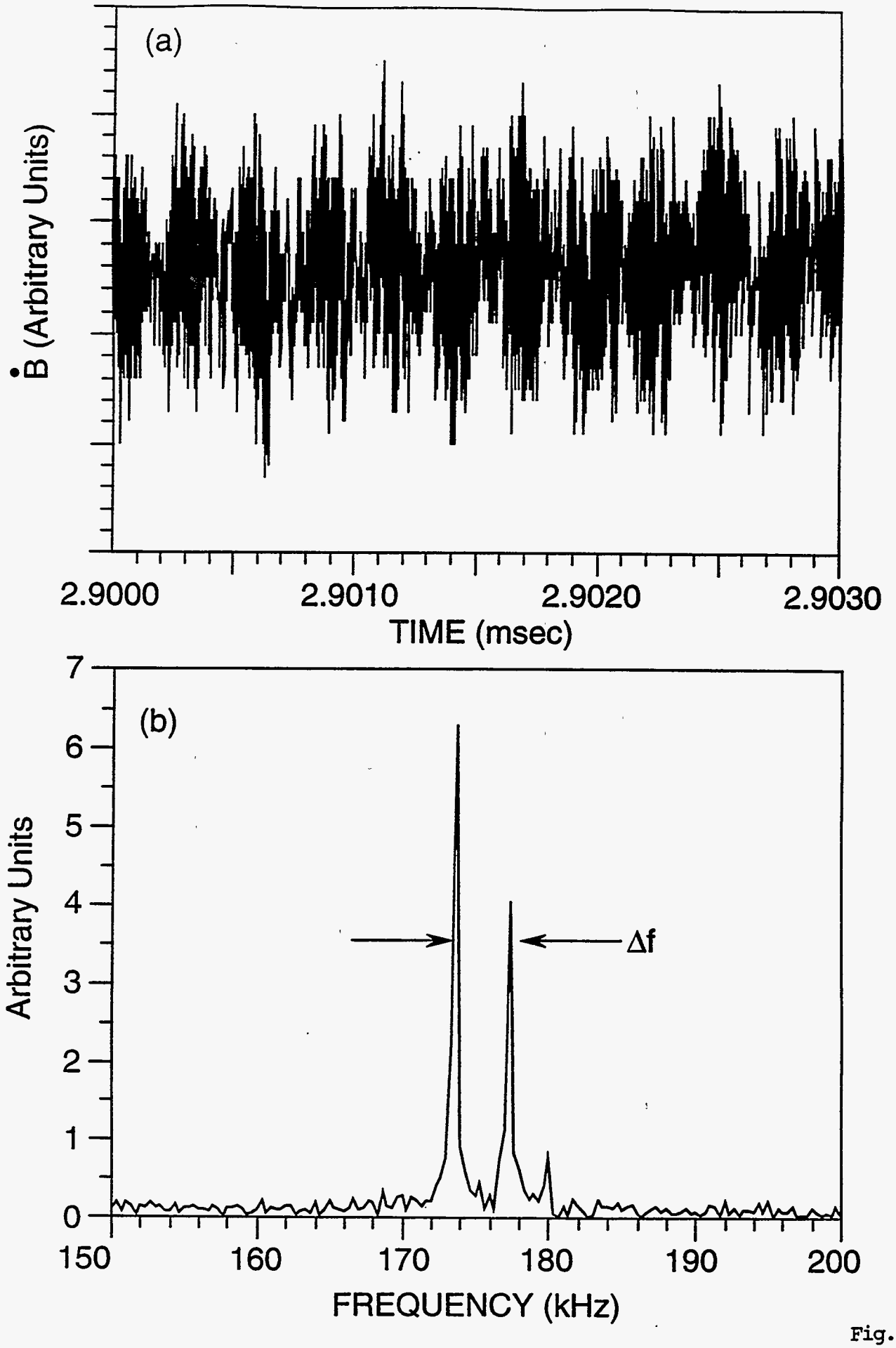
(a)
$\dot{B}$ (Arbitrary Units)
2.9000
2.9010
2.9020
2.9030
TIME (msec)
(b)
Arbitrary Units
0
1
2
3
4
5
6
7
Δf
150
160
170
180
190
200
FREQUENCY (kHz)

Fig. 6

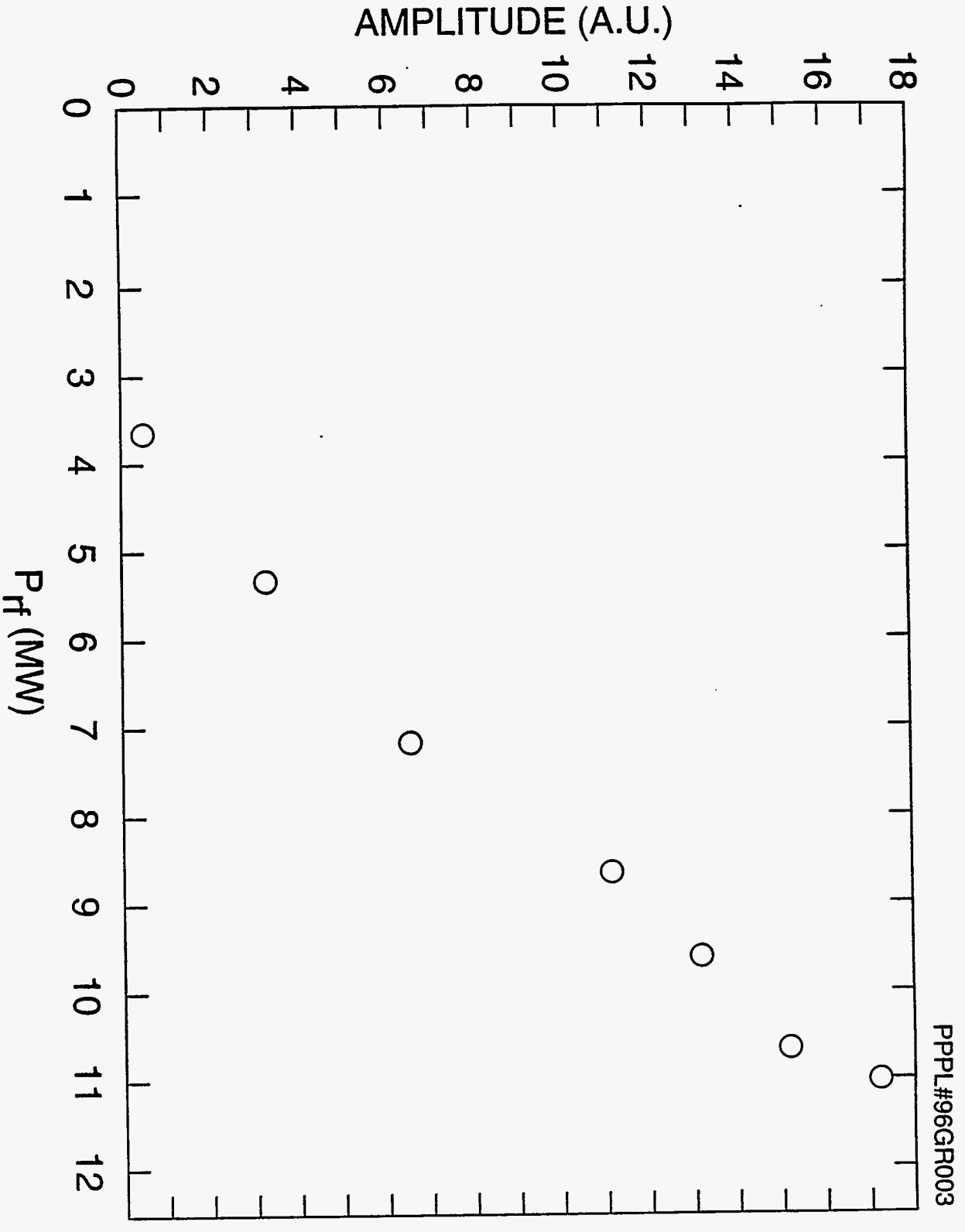
AMPLITUDE (A.U.)
0
2
4
6
8
10
12
14
16
18
P_{rf} (MW)
0
1
2
3
4
5
6
7
8
9
10
11
12
PPPL#96GR003

Fig. 7

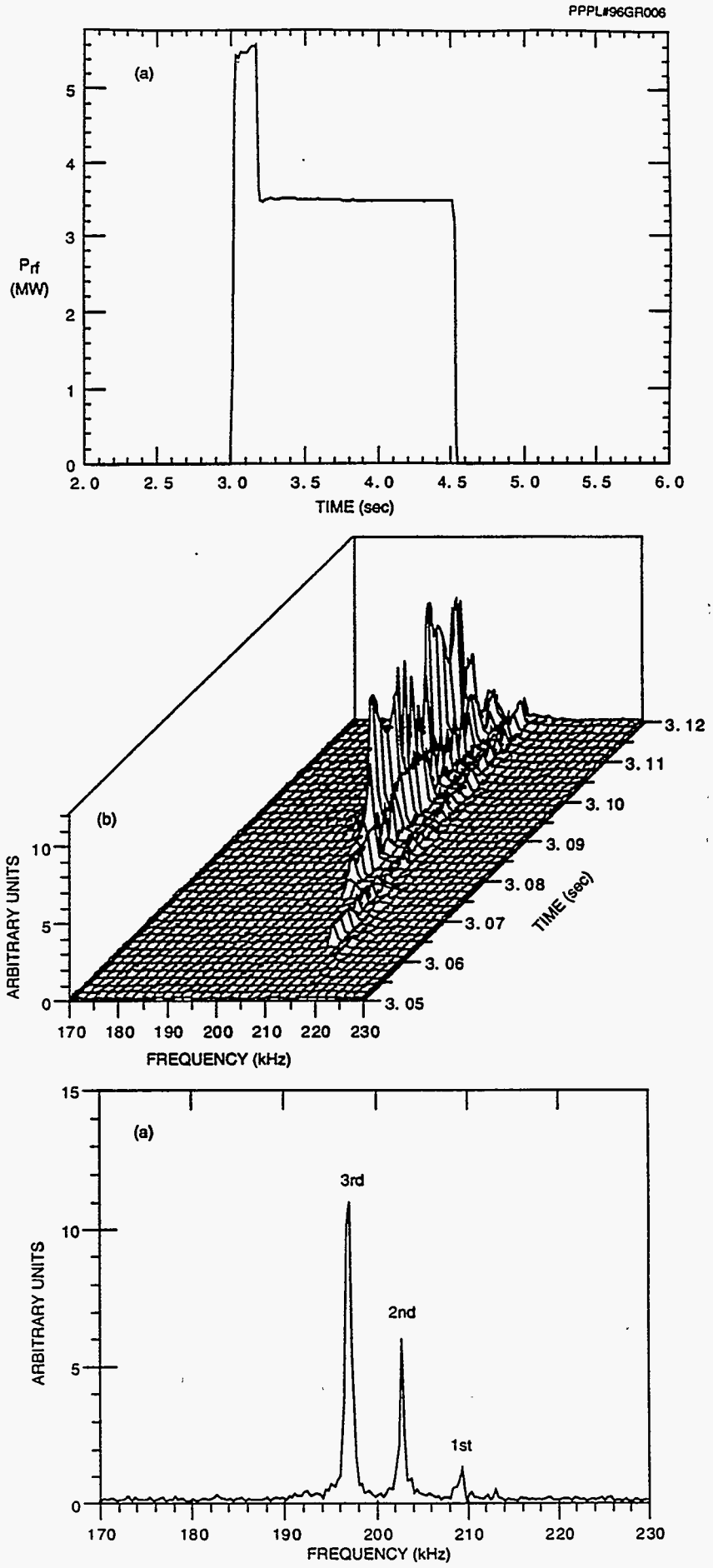
PPPL#96GR006
(a)
P_{rf} (MW)
TIME (sec)
(b)
ARBITRARY UNITS
FREQUENCY (kHz)
TIME (sec)
3.12
3.11
3.10
3.09
3.08
3.07
3.06
3.05
(a)
3rd
2nd
1st
ARBITRARY UNITS
FREQUENCY (kHz)

Fig. 8

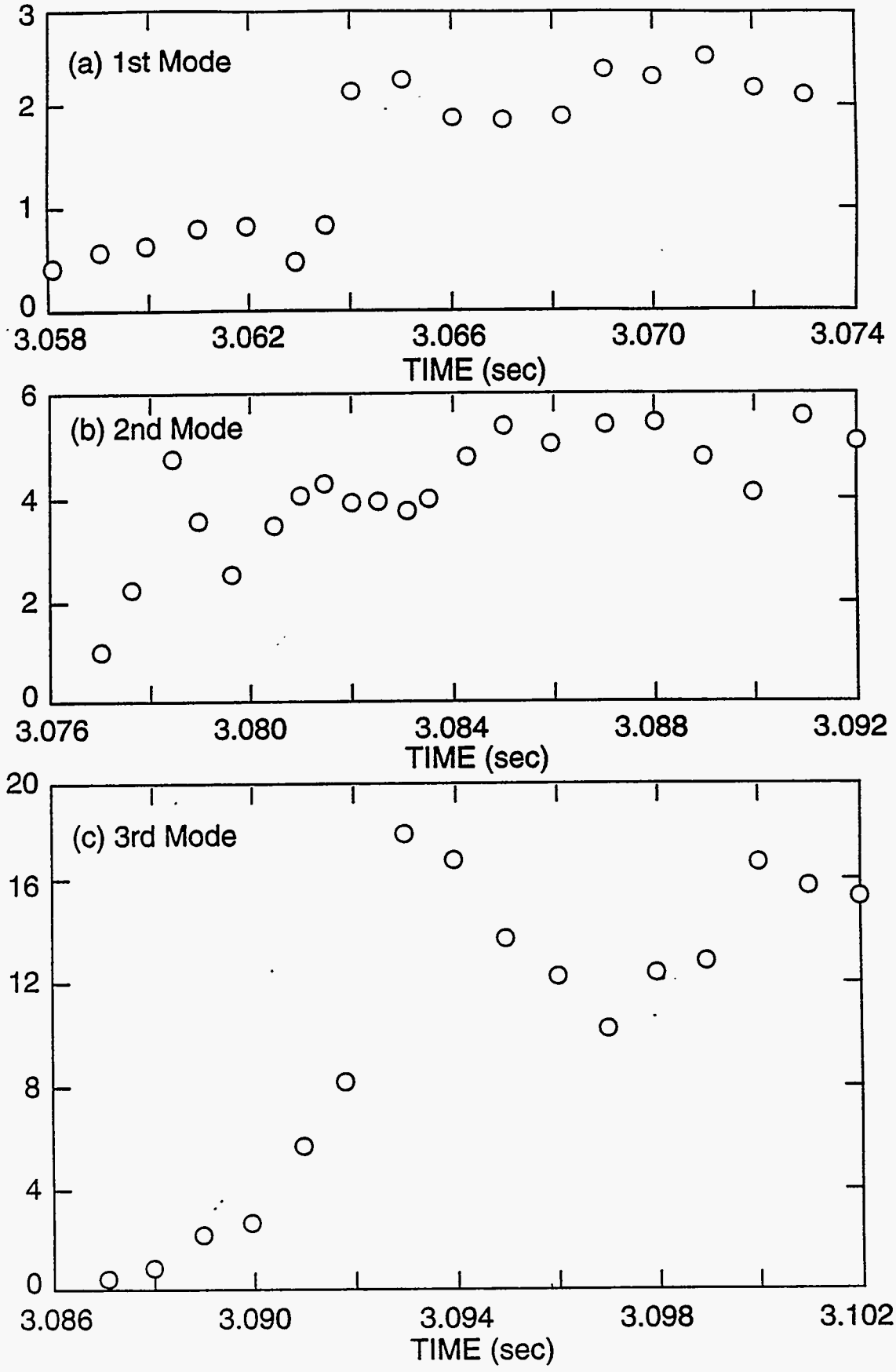
(a) 1st Mode
3
2
1
0
3.058
3.062
3.066
3.070
3.074
TIME (sec)
(b) 2nd Mode
6
4
2
0
3.076
3.080
3.084
3.088
3.092
TIME (sec)
(c) 3rd Mode
20
16
12
8
4
0
3.086
3.090
3.094
3.098
3.102
TIME (sec)

Fig. 9

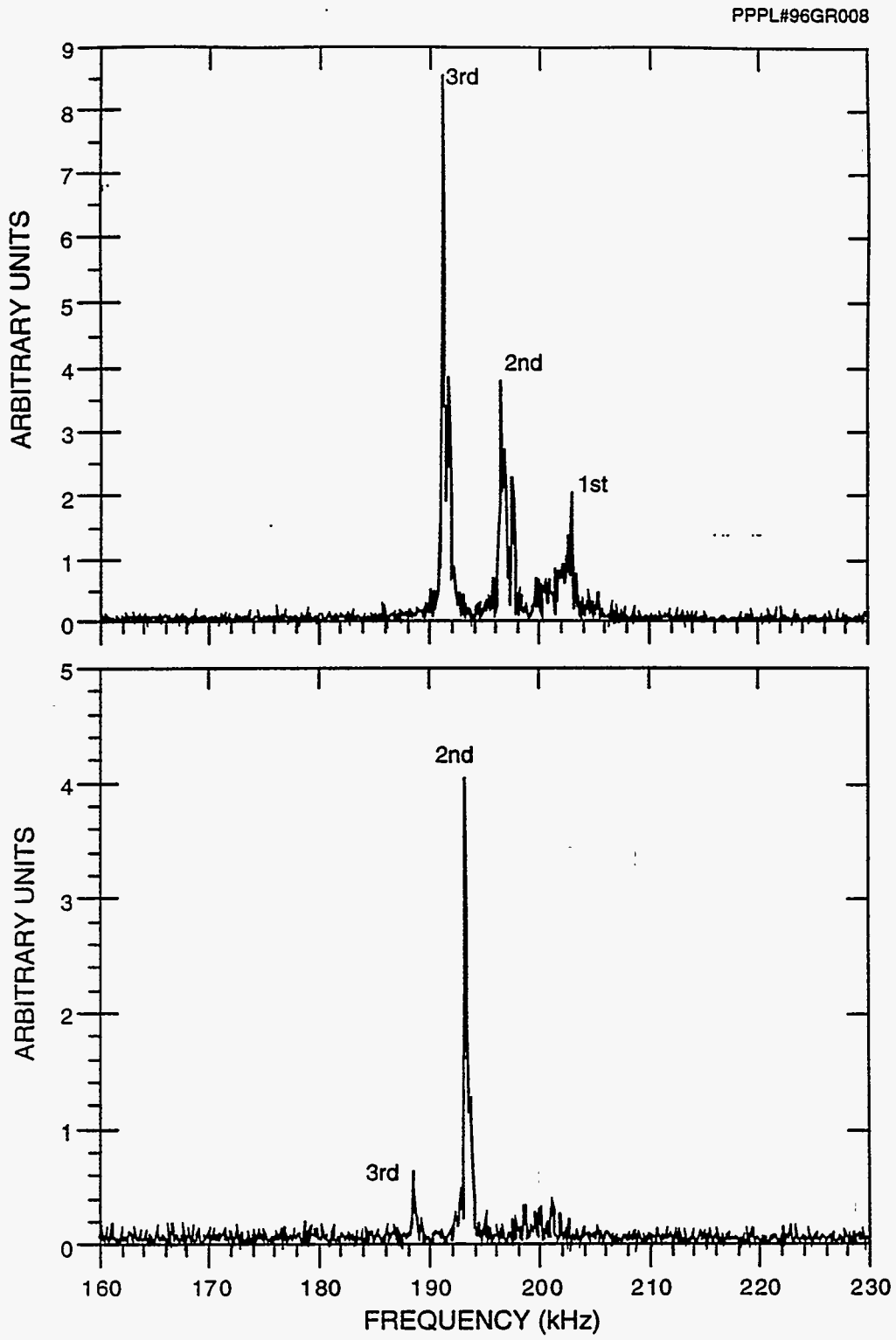
PPPL#96GR008
ARBITRARY UNITS
3rd
2nd
1st
ARBITRARY UNITS
2nd
3rd
FREQUENCY (kHz)

Fig. 10

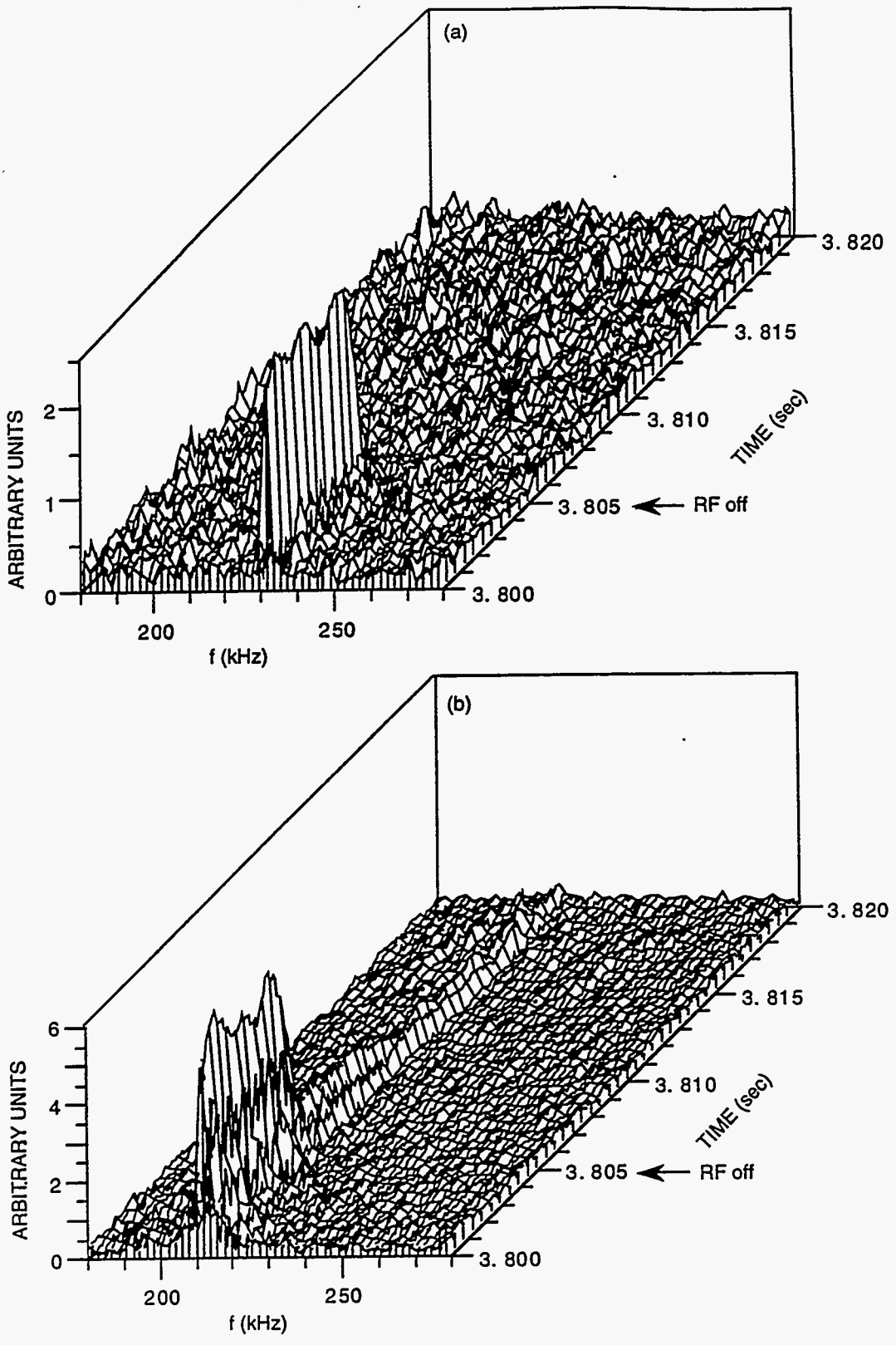
(a)
ARBITRARY UNITS
0
1
2
200
250
f (kHz)
3. 800
3. 805
RF off
3. 810
3. 815
3. 820
TIME (sec)
(b)
ARBITRARY UNITS
0
2
4
6
200
250
f (kHz)
3. 800
3. 805
RF off
3. 810
3. 815
3. 820
TIME (sec)

Fig. 11

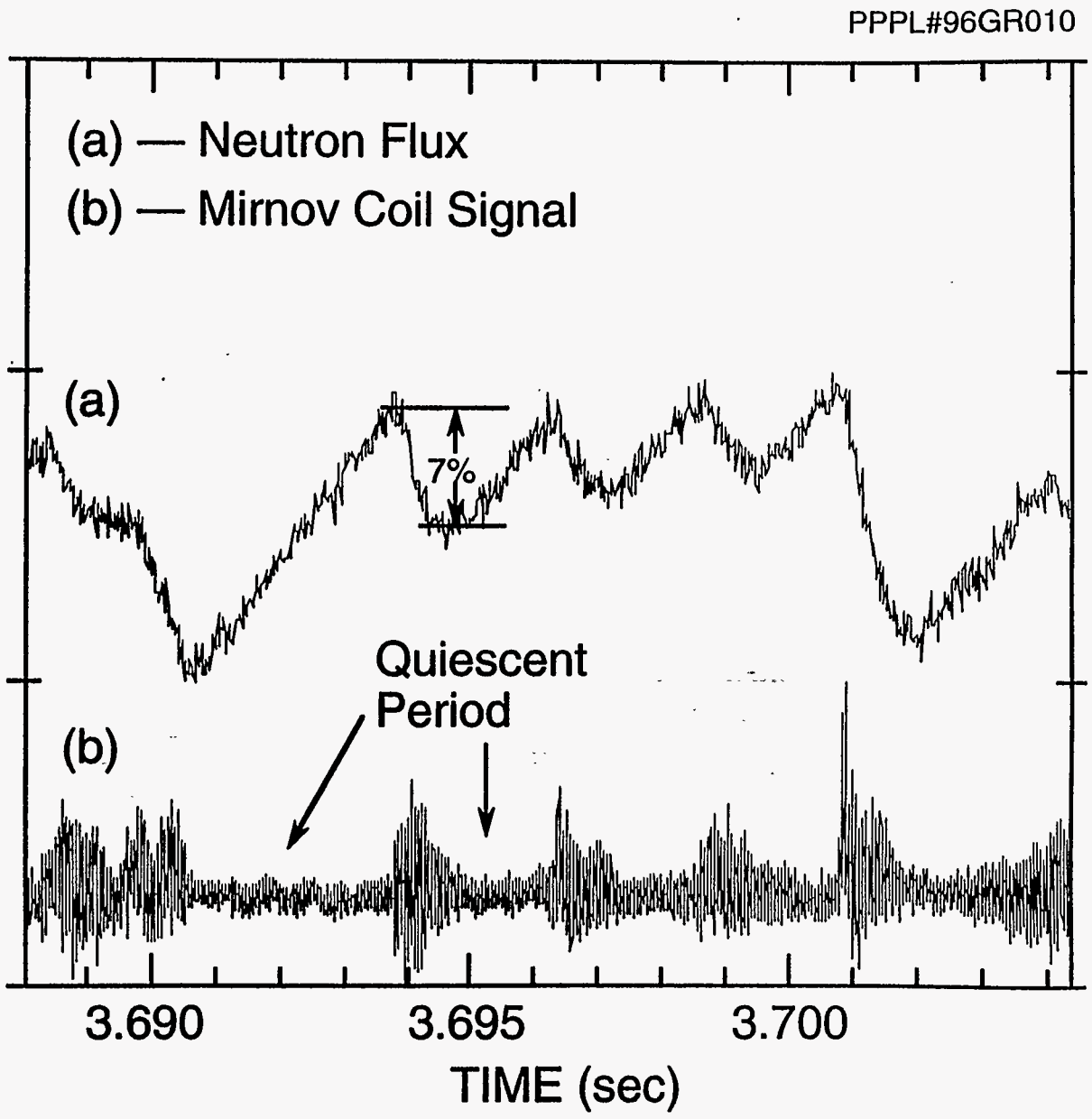
PPPL#96GR010
(a) — Neutron Flux
(b) — Mirnov Coil Signal
(a)
7%
Quiescent
Period
(b)
3.690
3.695
3.700
TIME (sec)

Fig. 12

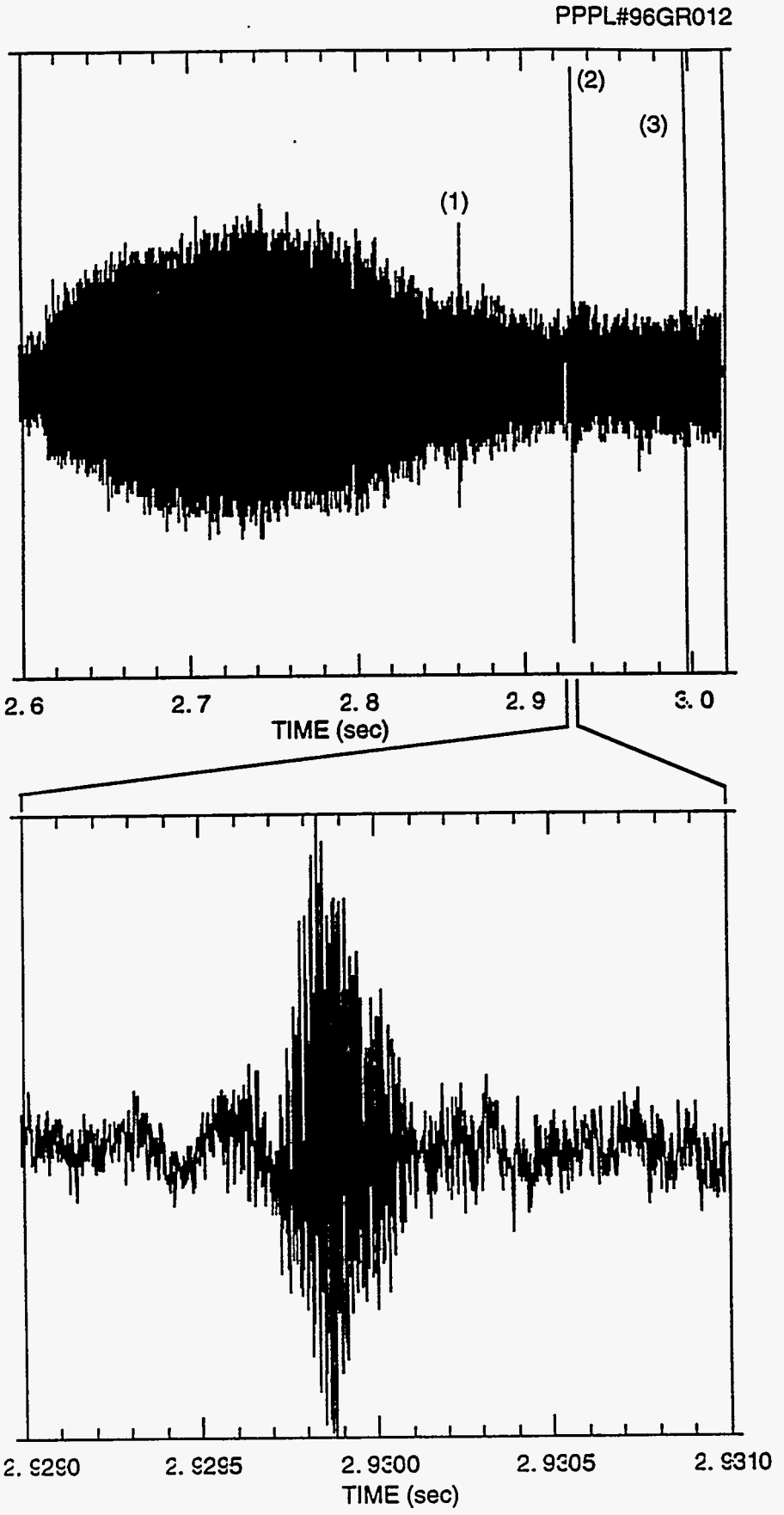
PPPL#96GR012
(1)
(2)
(3)
2.6
2.7
2.8
2.9
3.0
TIME (sec)
2.9290
2.9295
2.9300
2.9305
2.9310
TIME (sec)

Fig. 13

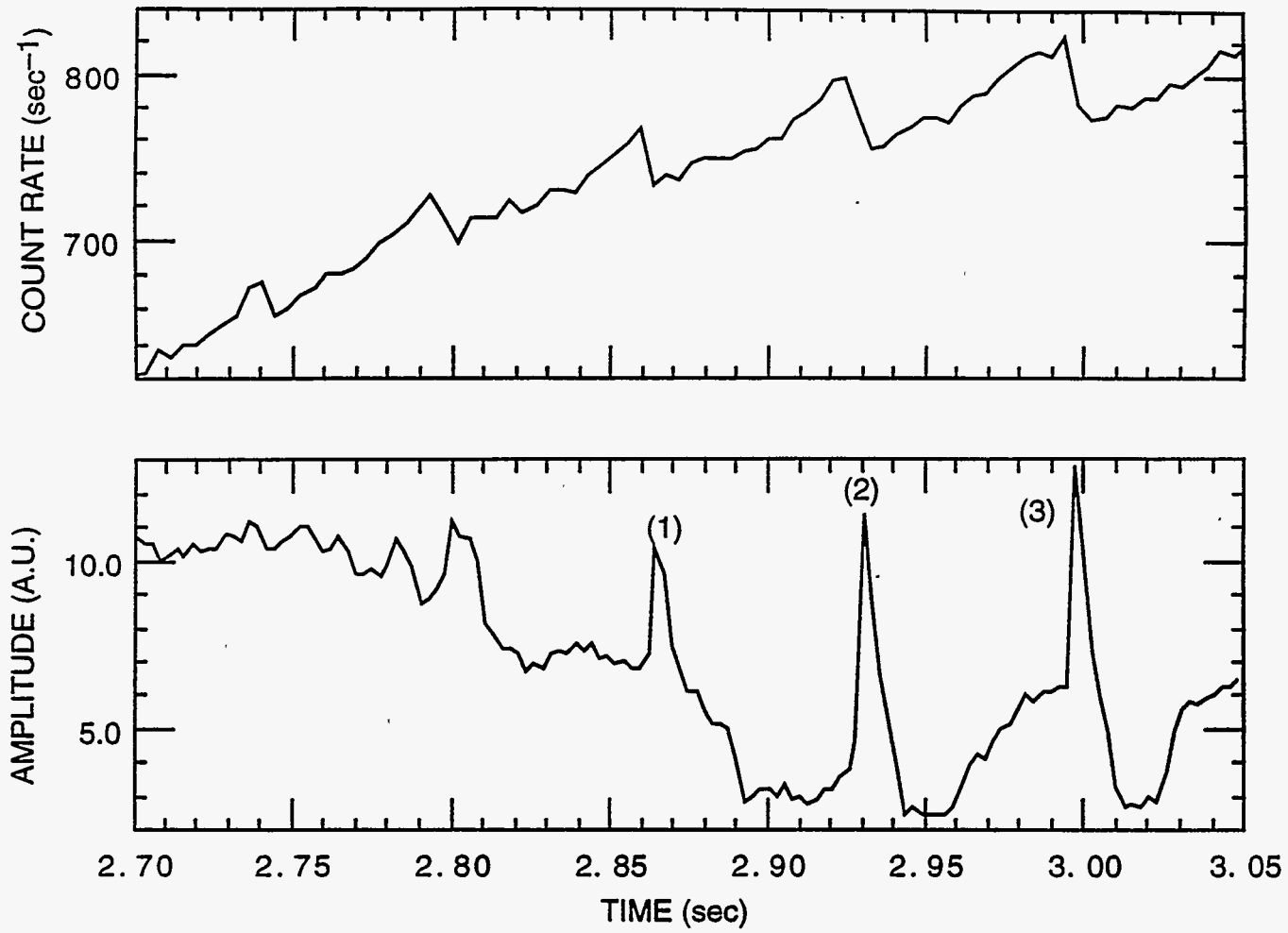
COUNT RATE (sec^{-1})
800
700
AMPLITUDE (A.U.)
10.0
5.0
(1)
(2)
(3)
2.70
2.75
2.80
2.85
2.90
2.95
3.00
3.05
TIME (sec)

Fig. 14